



1           **Projected Changes in Haze Pollution Potential in China: An**  
2                   **Ensemble of Regional Climate Model Simulations**

3

4                   Zhenyu Han<sup>1</sup>, Botao Zhou<sup>1,2</sup>, Ying Xu<sup>1</sup>, Jia Wu<sup>1</sup>, Ying Shi<sup>1</sup>

5           <sup>1</sup>National Climate Center, China Meteorological Administration, Beijing, China

6           <sup>2</sup> Collaborative Innovation Center on Forecast and Evaluation of Meteorological  
7           Disasters, Nanjing University of Information Science & Technology, Nanjing, China

8

9

10

11   **Corresponding author:** Botao Zhou

12   **Corresponding address:** National Climate Center, China Meteorological  
13   Administration, Beijing 100081, China

14   **E-mail:** zhoubt@cma.gov.cn



15 **Abstract.** Based on the dynamic downscaling by the regional climate model RegCM4  
16 from three CMIP5 global models under the historical and the RCP4.5 simulations, this  
17 article evaluated the performance of the RegCM4 downscaling simulations on the air  
18 environment carrying capacity (AEC) and weak ventilation days (WVD) in China,  
19 which are applied to measure haze pollution potential. Their changes during the  
20 middle and the end of the 21st century were also projected. The evaluations show that  
21 the RegCM4 downscaling simulations can generally capture the observed features of  
22 the AEC and WVD distributions over the period 1986-2005. The projections indicate  
23 that the annual AEC tends to decrease and the annual WVD tends to increase almost  
24 over the whole country except central China, concurrent with greater change by the  
25 late of the 21st century than by the middle of the 21st century. It suggests that annual  
26 haze pollution potential would be enlarged under the RCP4.5 scenario as compared to  
27 the present. For seasonal change in the four main economic zones of China, it is  
28 projected consistently that there would be a higher probability of haze pollution risk  
29 over the Beijing-Tianjin-Hebei (BTH) region and the Yangtze River Delta (YRD)  
30 region in winter and over the Pearl River Delta (PRD) zone in spring and summer in  
31 the context of the warming scenario. Over Northeast China (NEC), future climate  
32 change might reduce the AEC or increase the WVD throughout the whole year, which  
33 favors the occurrence of haze pollution and thus the haze pollution risk would be  
34 aggravated. Relative contribution of different components related to the AEC change  
35 further indicates that changes of the boundary layer depth and the wind speed play the  
36 leading roles in the AEC change over the BTH and NEC regions. In addition to those



37 two factors, the precipitation change also exerts dominant impacts on the ACE change

38 over the YRD and PRD zones.

39 **Keywords** air environment carrying capacity, ventilation day, haze pollution potential,

40 regional climate model, evaluation and projection

41



## 42 **1 Introduction**

43 Haze, as a phenomenon of severe air pollution, exerts remarkably adverse  
44 impacts on society and human health, thereby highly concerned by the public and  
45 policy makers. Particularly in recent years, heavy haze events hit China frequently  
46 (Wang et al., 2014; Zhang et al., 2014) and caused serious damages in many aspects.  
47 For instance, they not only increased traffic accidents and delayed traffic (Wu et al.,  
48 2005; 2008), but also aggravated ill health problems including respiratory disease,  
49 heart disease, cancer and premature death (Wang and Mauzerall, 2006; Xu et al.,  
50 2013). Thus, more and more attentions have been paid to the haze pollution in China.

51 The increasing trend of the haze days in China during recent decades (Ding and  
52 Liu, 2014; Song et al., 2014) is documented to be largely attributed to human  
53 activities. Due to rapid economic development and urbanization, the pollutants  
54 emitted into the atmosphere have been increased, consequently resulting in an  
55 intensification of haze pollution in China (Liu and Diamond, 2005; He et al., 2013;  
56 Wang et al., 2013b; 2016). Climate change also plays an important role (Jacob and  
57 Winner, 2009; Wang et al., 2016). Some studies have indicated that the reduction of  
58 surface wind speed, surface relative humidity and precipitation in recent decades (Gao,  
59 2008; Guo et al., 2011; Jiang et al., 2013; Song et al., 2014; Ding and Liu, 2014)  
60 provide unfavourable conditions for the sedimentation and diffusion of air pollutants,  
61 and thus increase the occurrence of haze pollution in China. Besides, the Arctic sea  
62 ice declining under global warming contributes positively to the increase of haze days  
63 in eastern China (Wang et al., 2015; Wang and Chen, 2016). Other influential climate



64 factors for the increase of haze pollution in China, such as the weakening of the East  
65 Asian winter monsoon (Li et al. 2015; Yin et al., 2015) and the northward shifting of  
66 the East Asian jet (Chen and Wang, 2015), are also highlighted. In summary, the  
67 combined effects of increased pollutants and climate change are responsible for the  
68 haze pollution in China.

69 IPCC AR5 reported that continued emissions of greenhouse gases will cause  
70 further changes in all components of the climate system (IPCC, 2013). From the point  
71 view of the CMIP5 projected change in climate conditions, there are both positive and  
72 negative contributors for the haze pollution in China. For example, the projected  
73 increase in precipitation (Xu and Xu, 2012; Tian et al., 2015; Wu et al., 2015b) is  
74 expected to reduce haze pollution, whereas the decrease of the Arctic sea ice extent  
75 (IPCC, 2013) and the weakening of the East Asian winter monsoon (Wang et al.,  
76 2013a) are inclined to increase haze pollution. So, how the haze pollution in China  
77 will change under the future warming scenario is still an open issue.

78 Air environment carrying capacity (AEC), which is a combined metric to  
79 measure atmospheric capacity in transporting and diluting pollutants into the  
80 atmosphere, provides a direct way to investigate the change of the haze pollution  
81 potential. When the AEC is low (high), it is unfavourable (favourable) for the  
82 diffusion and cleaning of the pollutants, and thus the haze pollution is (not) prone to  
83 occur. So far, the AEC has been applied in the operation of China Meteorological  
84 Administration (CMA) to forecast haze pollution potential (Kang et al., 2016). On the  
85 other hand, CMIP5 global models show some limitations in simulating regional



86 climate due to their relatively coarse resolutions (Giorgi et al., 2009). Regional  
87 climate models with higher resolutions are demonstrated to outperform global models  
88 on the regional scale (Lee and Hong 2014; Wu et al. 2015a; Gao et al. 2012, 2016b).  
89 Thus, this study is aimed to project changes of the haze pollution potential in China  
90 from the AEC perspective, based on the downscaling simulations of the regional  
91 climate model RegCM4 under the RCP4.5 scenario.

92

## 93 **2 Model, data and method**

### 94 **2.1 Data, regional climate model and simulations**

95 The regional climate model RegCM4 used in this study is developed by the ICTP  
96 (Giorgi et al., 2012) and applied widely around the world. The model has the  
97 horizontal resolution of 25 km and 18 vertical sigma layers with the top at 50 hPa.  
98 Based on the study of Gao et al. (2016a, b), we selected a suite of physical  
99 parameterization schemes suitable for the simulation of China climate, including the  
100 Emanuel convection scheme (Emanuel, 1991), the radiation package of the CCM3  
101 model for atmospheric radiative transfer (Kiehl et al., 1998), the non-local formulation  
102 of Holtslag (Holtslag et al., 1990) for planetary boundary layer, the SUBEX  
103 parameterization for large-scale precipitation (Pal et al., 2000), and the CLM3.5 for  
104 land surface process (Oleson et al., 2008). The land cover data were updated based on  
105 the vegetation regionalization maps of China (Han et al., 2015).

106 The domain for the downscaling simulations is the region recommended by  
107 CORDEX-East Asia phase II (Giorgi et al., 2009), covering China continent and



108 adjacent regions. The RegCM4 simulations, called EC, HAD, and MPI for short, were  
109 driven at 6-hourly intervals by the historical (1979-2005) and RCP4.5 (2006-2099)  
110 simulations from three CMIP5 global models i.e., EC-EARTH, HadGEM2-ES, and  
111 MPI-ESM-MR, respectively. The average of the three simulations with equal weight  
112 is taken as the ensemble mean. The historical simulation denotes the past climate, and  
113 the RCP4.5 represents the medium-low radiative forcing scenario with the radiative  
114 forcing peaking at  $4.5 \text{ Wm}^{-2}$  by 2100 (Taylor et al., 2012). Readers can visit  
115 <http://cmip-pcmdi.llnl.gov/cmip5> for the information about the three CMIP5 models  
116 and the forcing.

117 To validate the performance of the RegCM4 downscaling simulations, the  
118 ERA-Interim reanalysis dataset (Uppala et al., 2008) with the horizontal resolution of  
119  $1.5^\circ \times 1.5^\circ$  was employed as observations, including 6-hourly boundary layer height,  
120 precipitation, geopotential height and wind speed.

## 121 2.2 Analysis method

122 The AEC considers the processes of wet deposition and ventilation and is  
123 expressed in the form:

$$124 \quad \text{AEC} = C_s \cdot (W_r \cdot R \cdot \sqrt{S} + \frac{\sqrt{\pi}}{2} \cdot U_{BL} \cdot H) \quad (1)$$

125 where  $C_s$  is the standard concentration of air pollutant (here, the value is  $75 \mu \text{g m}^{-3}$ ,  
126 standard concentration for  $\text{PM}_{2.5}$  in China),  $W_r$  is washout constant ( $6 \times 10^5$ ),  $R$  is  
127 precipitation,  $S$  is unit area and defined as  $2500 \text{ km}^2$ ,  $U_{BL}$  is mean wind speed  
128 averaged within the boundary layer,  $H$  is boundary layer height (Xu and Zhu, 1989).  
129 High (Low) AEC is disadvantageous (advantageous) for the occurrence of haze



130 pollution, indicating low (high) haze pollution potential. It should be pointed out that  
 131 the AEC measures atmospheric carrying capacity in transporting and diluting  
 132 pollutants. It does not reflect real emission characteristics. The  $C_s$  is the standard  
 133 concentration of air pollutant not the real concentration of the pollutant emitted into  
 134 the air. For different pollutants, different value can be fixed for  $C_s$ . Because what we  
 135 concerned in this study is the haze pollution potential, its value is set as the standard  
 136 concentration for  $PM_{2.5}$  in China.

137 The term  $U_{BL} \cdot H$  is named ventilation coefficient (Krishnan and Kunhikrishnan,  
 138 2004). Large ventilation coefficient means that a deeper boundary layer can dilute  
 139 pollutants and strong winds can remove local pollutants, unfavourable for the haze  
 140 occurrence, and vice versa. If each of the 6-hourly ventilation coefficients within one  
 141 day is less than  $6000 \text{ m}^2 \text{ s}^{-1}$ , this day is counted as one weak ventilation day (WVD)  
 142 (Leung and Gustafson, 2005). Longer WVD indicates more haze pollution incidents.

143 According to Eq. (1), the AEC change results from changes in precipitation,  
 144 wind speed, and boundary layer depth, which can be simplified as:

$$145 \quad \Delta AEC = \alpha \cdot \Delta R + \beta \cdot \Delta(U_{BL} \cdot H) \quad (2)$$

146 where  $\alpha = C_s \cdot W_r \cdot R$ ,  $\beta = C_s \cdot \frac{\sqrt{\pi}}{2}$ , and  $\Delta$  represents the difference between the future and  
 147 present-day climate (RCP4.5 minus reference period).

148 The Eq. (2) could be further decomposed as follows:

$$149 \quad \Delta AEC = \alpha \cdot \Delta R + \{\beta \cdot \Delta U_{BL} \cdot H_{pd} + \beta \cdot (U_{BL})_{pd} \cdot \Delta H + \beta \cdot \Delta U_{BL} \cdot \Delta H + TR\} \quad (3)$$

150 The subscript “pd” denotes the present-day climate. The first to third terms in the  
 151 right-hand side are associated with changes in precipitation, wind speed within the





152 boundary layer, and boundary layer depth, respectively. The fourth term is a nonlinear  
153 term including the contribution of changes in both wind speed and boundary layer  
154 depth. Since we use 6-hourly data for the AEC calculation while monthly mean data  
155 for the diagnosis of the change, the last term TR (transient term, deviation from  
156 monthly mean) cannot be ignored, which is obtained as a residual.

157 The pattern-amplitude projection (PAP) method (Park et al., 2012) is applied to  
158 quantify the relative contributions of individual processes  $P_i$  to the AEC change over  
159 certain region.

$$160 \quad P_i = \frac{\langle \Delta AEC_i \cdot \Delta AEC \rangle}{\langle \Delta AEC \cdot \Delta AEC \rangle} \quad (4)$$

161 in which  $\langle \rangle$  represents area mean,  $\Delta AEC_i$  represents components in the  
162 right-hand side of Eq. (3).

163

### 164 **3 Performance of the downscaling simulations**

165 The performance of the RegCM4 downscaling simulations on the AEC spatial  
166 pattern is firstly evaluated through the comparison with the observation. As shown in  
167 Fig. 1a, the observed AEC is in general large in western China, with the maxima  
168 located over Tibet. Low AEC is found mainly over central and eastern China,  
169 northwestern Xinjiang, and parts of Northeast China. The simulated AEC  
170 distributions from the ensemble (Fig. 1b) and its members (Fig. 1c-e) show general  
171 resemblance to the observation. The spatial correlation coefficients between the  
172 simulation and the observation are all higher than 0.75 (Table 1). On the national  
173 average, the root mean square error (RMES) is small for the ensemble mean and each



174 member, which varies between 0.47 and 0.54 (Table 1). Nevertheless, there are also  
175 some deficits in the simulations. For example, the AEC is underestimated over the  
176 southern Xinjiang and overestimated over parts of North China.

177 We further present the observed and simulated distribution of the seasonal AEC  
178 in China during 1986-2005. For the observation, the winter AEC is the lowest among  
179 the four seasons in a broad region of China (Fig. 2a). In spring, the AEC increases  
180 significantly and the regions with high AEC expand obviously. The central eastern  
181 China is dominated by the low capacity (Fig. 2c). Compared with the case in spring,  
182 the summer AEC increases over central China while decreases slightly over Tibet and  
183 Northeast China (Fig. 2e). The AEC distribution in autumn is similar to that in winter  
184 but with larger capacity over the regions except Tibet (Fig. 2g). The seasonal  
185 variation of the AEC in the ensemble simulation agrees with that in the observation  
186 although there are some discrepancies (Fig. 2b, 2d, 2f and 2h). The spatial correlation  
187 coefficient between the simulation and the observation ranges from 0.61 to 0.79 and  
188 the RMES is in the range of 0.47 to 0.76 for the national average in four seasons  
189 (Table 2).

190 The WVD distribution during 1986-2005 in the observation and the ensemble  
191 simulation is displayed in Fig. 3a and Fig.3b, respectively. It is noticed that the  
192 simulated pattern and the observed pattern are approximate to each other. Namely, the  
193 number of weak ventilation days per year is relatively small over Tibet while  
194 relatively large over central and eastern China, Northeast China, southern North



195 China and Xinjiang. The spatial correlation between them is 0.74. However, we also  
196 note that the WVD is overestimated by the ensemble simulation.

197 The wet deposition is observed to be large over southern China and the south  
198 edge of the Tibetan Plateau while small over northwestern China (Fig. 3c). According  
199 to Eq. (1), the wet deposition pattern exactly corresponds to the distribution of  
200 precipitation. The observed features can also be captured by the ensemble simulation  
201 (Fig. 3d). The spatial correlation coefficient between the simulation and the  
202 observation is up to 0.84.

203 In brief, the downscaling simulations of the RegCM4 can reasonably reproduce  
204 the observed characteristics of the distribution of the AEC, WVC and wet deposition  
205 in China. It provides justification to use them for the future projection.

206

#### 207 **4 Projected changes**

208 Fig. 4 exhibits the ensemble projected changes in AEC, WVC and wet deposition  
209 during the middle of the 21st century (2046-2065) and the end of the 21st century  
210 (2080-2099) relative to the reference period 1986-2005. A general decrease in AEC  
211 and an overall increase in WVC are projected over almost the whole country except  
212 central China in the context of the RCP4.5 scenario. The change in magnitude is  
213 larger by the end of the 21st century than by the middle of the 21st century. The  
214 maximum decrease in AEC appears at the edge of the Qinghai-Tibet Plateau and the  
215 Loess Plateau, with the percentage change being 4% for the middle of the 21st  
216 century and 5% for the end of the 21st century. The relatively large decreases are



217 located in Southwest China, northern North China, Northeast China and Inner  
218 Mongolia (Fig. 4a and Fig.4b). The increase in WVD is projected to be particularly  
219 pronounced in western and northern China (Fig. 4c and Fig. 4d). The three ensemble  
220 samples agree well on the sign of the changes, indicative of a good consistency in the  
221 projection. In contrast, there would be an increasing tendency for the AEC and a  
222 decreasing tendency for the WVD over central China where the climatological  
223 capacity is low in the reference period 1986-2005. However, the sign of the projected  
224 change is inconsistent among the three ensemble samples. Compared with the  
225 ensemble projection, the EC and HAD show relatively large discrepancy for the sign  
226 of the projected change in AEC and WVD, respectively (Figures not shown).

227 For the change in wet deposition, a general increase is projected across China,  
228 also with greater change in 2080-2099 than in 2046-2065 (Fig. 4e and Fig. 4f). In  
229 addition, we can find inconsistent signs of the projected change over southern China  
230 during 2046-2065 (Fig. 4e) and over some parts of Northeast China during 2080-2099  
231 (Fig. 4f). The inconsistent during 2046-2065 (2080-2099) is mainly due to the  
232 difference of the HAD (MPI) projection from the other two ensemble members  
233 (Figures not shown).

234 Following, we turn to examine the seasonal and annual changes of the AEC and  
235 WVD over the four main economic zones of China which suffer severely from the  
236 haze pollution at present, i.e., Beijing-Tianjin-Hebei region (BTH), Northeast China  
237 (NEC), Yangtze River Delta economic zone (YRD), and Pearl River Delta economic  
238 zone (PRD) in more detail.



## 239 1) Beijing-Tianjin-Hebei region

240 As shown in Fig. 5a, the ensemble projection indicates a decrease of the AEC in  
241 all four seasons during the middle of the 21st century. The percentage change relative  
242 to 1986-2005 is the lowest in spring and the largest in winter. The changes in summer  
243 and autumn are between -2% and -3%. The three ensemble members agree on the sign  
244 of the changes in all seasons except spring but with different spread. For the summer  
245 season, the spread is the smallest. While in other seasons, it is close to or larger than  
246 the ensemble projected change. During the end of the 21st century, the decrease of the  
247 AEC is further enhanced, with the largest enhancement occurring in winter. Moreover,  
248 the spread in general becomes much larger. For annual change, both the ensemble and  
249 its members project that the AEC would reduce during the middle and the end of the  
250 21st century with the larger amplitude in the latter period.

251 As for the WVD (Fig. 5b), an increasing tendency is projected by the ensemble  
252 for annual and seasonal mean during the middle of the 21st century. The change is the  
253 smallest in summer and the largest in winter. The ensemble members show good  
254 agreement on the positive change in winter, autumn, and annual mean. During the late  
255 of the 21st century, the increase in WVD is further enlarged in winter and autumn  
256 while it is reduced in spring and summer. There is no appreciable change for annual  
257 mean as compared to that in the middle of the 21st century. Only for the winter season  
258 and annual mean, all the individual simulations consistently show the same projection  
259 as the ensemble.



## 260 2) Northeast China

261 The annual and seasonal AEC is projected by the ensemble to decrease during  
262 the middle of the 21st century, and the percentage changes are comparable among  
263 four seasons and annual mean (Fig. 6a). The ensemble members also project negative  
264 tendency consistently except in spring. Compared with the middle of the 21st century,  
265 the case for the end of the 21st century is similar but with larger decrease. Besides, all  
266 the three ensemble members show good consistence for the projection.

267 The WVD is projected by the ensemble and its members to increase during the  
268 middle and the end of the 21st century for annual mean and all four seasons (Fig. 6b).  
269 Similarly, the projected change is larger during the end of the 21st century than during  
270 the middle of the 21st century, with the largest increase appearing in spring.

## 271 3) Yangtze River Delta economic zone

272 The ensemble projection indicates that the AEC would decrease for annual mean  
273 and all the seasons except autumn (Fig. 7a). The percentage change is the smallest in  
274 spring (with the decrease of less than 1%) and the greatest in winter (with the  
275 decrease of more than 3%). The counterparts for summer and autumn are about -2%  
276 and 1%, respectively. However, large spread exists among the projections of the three  
277 ensemble members. Only for winter and annual mean, they project the same sign of  
278 the change. At the end of the 21st century in the ensemble projection, the decrease in  
279 AEC is enhanced to 6% in winter. Consistent change is projected by the ensemble  
280 members. In contrast, the decrease in summer and the increase in autumn are  
281 weakened as compared to the middle of the 21st century. A slight increase of the AEC



282 is found in spring. For annual mean AEC, the decrease is somewhat larger by the end  
283 of the 21st century than by the middle of the 21st century.

284 The WVD for annual mean, winter and spring is projected by the ensemble to  
285 increase, with larger change during the end of the 21st century than during the middle  
286 of the 21st century (Fig. 7b). The greatest change occurs in winter. For summer, the  
287 ensemble projects that the WVD almost remains unchanged during the middle of the  
288 21st century while increases at the end of the 21st century. For autumn, the ensemble  
289 projects that the WVD decreases slightly during the middle of the 21st century while  
290 increases slightly by the end of the 21st century. The ensemble members show good  
291 consistency of the projections for winter and annual mean during both periods.

#### 292 4) Pearl River Delta economic zone

293 As projected by the ensemble (Fig. 8a), the annual, spring and summer AEC  
294 would decrease. Such a decrease is relatively larger during the middle of the 21st  
295 century than during the end of the 21st century and the greatest decrease occurs in  
296 spring. For winter, the AEC is projected to increase and be comparable during the  
297 middle and the end of the 21st century. For autumn, the projected AEC decreases by  
298 about 1% over the period 2046-2065 and increase by about 0.5% over the period  
299 2080-2099. However, the projections from the three members are not consistent for  
300 all four seasons.

301 The ensemble projects an increase in WVD for annual mean and four seasons,  
302 with the greatest increase in summer during the middle of the 21st century (Fig. 8b).  
303 The individual members consistently show the positive change for spring, summer,



304 and annual mean. Compared with the middle of the 21st century, the increase of the  
305 WVD is reduced in summer while enhanced for annual mean and the remaining  
306 seasons during the late of the 21st century. The autumn is the season with the  
307 maximum change. The individual members show the same projections as the  
308 ensemble on the sign of change still for spring, summer, and annual mean.

309 The consistence of the three ensemble members on the direction of the projected  
310 change which can be used to visualize the uncertainty in the projection is further  
311 summarized in Table 3. In general, although there are some uncertainties on the  
312 regional changes, the three members consistently project a decrease of the AEC or an  
313 increase of WVD for annual mean over the four economic zones, especially over the  
314 Beijing-Tianjin-Hebei region and Northeast China. It signifies that future climate  
315 change will contribute positively to the haze pollution in these regions. For seasonal  
316 change, decrease in AEC or increase in WVD, is projected consistently to appear in  
317 all four seasons over Northeast China. It suggests that there would be an increase of  
318 haze pollution potential throughout the whole year. Besides, the consistent projections  
319 indicate a higher potential risk of haze pollution over the Beijing-Tianjin-Hebei  
320 region and the Yangtze River Delta region in winter and over the Pearl River Delta  
321 zone in spring and summer.

322 The temporal evolution of the annual and seasonal AEC and WVD over the four  
323 main economic zones are also plotted (Figs. 5-8 c-g), and the corresponding trend  
324 values projected by the ensemble for the period of 2016-2099 are summarized in  
325 Table 4. Theil-Sen trend analysis (Theil, 1950; Sen, 1968) was used to estimate the





326 trends and the non-parametric Mann-Kendall test (Mann, 1945; Kendall, 1975) was  
327 used for significant test. Generally, the secular variations of the AEC and the WVD  
328 show some diversity across different seasons over the regions except NEC where a  
329 decrease in AEC and an increase in WVD is projected uniformly. Nevertheless, for  
330 the trends significant above the 95% level, it is interesting to notice that the decrease  
331 in AEC is mostly accompanied with the increase in WVD, for instance for winter over  
332 TBH, for annual mean and all the seasons over NEC, for annual mean, winter and  
333 summer over YRD, and for annual mean and autumn over PRD.

334

### 335 **5 Contributions of different factors to the change of AEC**

336 Based on Eqs. (2) and (3), we further investigate the contribution of different  
337 factors to the projected change in AEC. For brevity, we only show the results for the  
338 period 2046-2065 in the following, because the case for the period 2080-2099 is  
339 similar.

340 Figs. 9a and 9b exhibit relative contributions to the annual AEC change over the  
341 course of 2046-2065 from changes in precipitation and ventilation, respectively.  
342 Overall, the ventilation change plays a dominant role in and contributes positively to  
343 the change of the AEC over most parts of China, particularly in western and northern  
344 China (Fig. 9b). In contrast, the relative contribution of the precipitation change is in  
345 general negative over western and northern China while positive over southern China  
346 (Fig. 9a).



347           According to Eq. (3), the effect of ventilation change can be decomposed into  
348   four terms, i.e., wind speed change, boundary layer depth change, nonlinear term, and  
349   transient term. Among these contributors for annual ventilation change, the effects of  
350   boundary layer depth (Fig.9d) and wind speed (Fig.9c) are relatively large and the  
351   former is greater than the latter over most parts of eastern China. The transient term  
352   also exert effects for instance over some parts of western and southern China (Fig.9f),  
353   while the effects of the nonlinear term are tiny across China (Fig. 9e).

354           Fig. 10 further presents relative contributions of aforementioned factors to  
355   annual and seasonal AEC change over the four economic zones as projected by the  
356   ensemble and its members. As shown in Figs. 10a and 10b, changes in wind speed  
357   and boundary layer depth have the greatest contributions to the AEC change over the  
358   THB and NEC regions for annual mean and all the seasons except summer. The  
359   contribution from the precipitation is in general relatively small. Besides, the effects  
360   of the transient term are larger than that of the precipitation, and the effects of the  
361   nonlinear term can be negligible. These results indicate that changes in wind speed  
362   and boundary layer depth are the leading contributors responsible for the AEC change  
363   over the two regions. In contrast, over the YRD (Fig.10c) and PRD (Fig.10d) zones,  
364   change in precipitation also plays a dominant role. The contribution from the  
365   precipitation change is comparable to and even larger than that from changes in wind  
366   speed and boundary layer depth for all the seasons except winter.

367



## 368 **6 Conclusion**

369 In this study, we conducted downscaling simulations by use of the RegCM4  
370 driven by three CMIP5 models' results under the historical simulation and the RCP4.5  
371 scenario. On this basis, we evaluated the fidelity of the RegCM4 simulations on the  
372 AEC and WVD which are indicators for haze pollution potential, and then projected  
373 their change during the middle and the end of this century for China and four main  
374 economic zones. The major findings are summarized below:

375 1) The evaluation indicates that the RegCM4 downscaling simulations in general  
376 show good performance in modeling the climatological distribution of the annual and  
377 seasonal AEC, despite some discrepancies in certain regions. The spatial correlations  
378 between the simulation and the observation for annual mean and four seasons are  
379 higher above 0.6. The simulations also well capture the observed WVD pattern with  
380 relatively small WVD over Tibet and relatively large WVD over central and eastern  
381 China, Northeast China, southern North China and Xinjiang, although the WVD is  
382 overestimated systematically.

383 2) The annual AEC and WVD are respectively projected by the ensemble to  
384 decrease and increase almost in the entire region except central China, accompanied  
385 with larger amplitude by the end of the 21st century than by the middle of the 21st  
386 century. The decreases in AEC are relatively large over Tibet, Southwest China,  
387 northern North China, Northeast China and Inner Mongolia. The increase in WVD is  
388 particularly pronounced in northern China. The individual members present consistent  
389 projections of changes as the ensemble. In contrast, the ensemble projects an increase



390 in AEC and a decrease in WVD over central China. However, the sign of the  
391 projected change is inconsistent among the ensemble samples.

392 3) The consistency analysis suggests that there would be a high probability of the  
393 increase in air pollution risk over the BTH and YRD regions in winter and over the  
394 PRD zone in spring and summer in a warmer world. Over NEC, climate change might  
395 reduce the AEC or increase the WVD throughout the whole year, favorable for the  
396 occurrence of haze pollution and also indicative of an aggravation of haze pollution  
397 risk. Furthermore, the contribution analysis indicates that changes in boundary layer  
398 depth and wind speed play the leading roles in the AEC change over the BTH and  
399 NEC regions. In addition to the aforementioned two factors, the precipitation change  
400 is also a dominant factor influencing the ACE change over the YRD and PRD zones.

401 In this study, we mainly showed the downscaled results driven by three global  
402 models. Note that the planetary boundary layer depth is not a standard CMIP5 output  
403 variable, and the coarse vertical resolution of the global models prevents us from  
404 estimating the planetary boundary layer depth. Moreover, the CMIP5 experiments did  
405 not supply high-frequency (six-hourly) outputs for calculating AEC and WVD. These  
406 make it hard to estimate whether the consistencies and inconsistencies of the  
407 projection is caused by the global models or to some extent affected by the dynamical  
408 downscaling of the regional model.

409



410 **Acknowledgments.** This research was jointly supported by the National Key  
411 Research and Development Program of China (2016YFA0600701), the National  
412 Natural Science Foundation of China (41675069, 41405101), and the Climate Change  
413 Specific Fund of China (CCSF201626).



414 **References**

- 415 Chen, H. P. and Wang, H. J.: Haze days in North China and the associated  
416 atmospheric circulations based on daily visibility data from 1960 to 2012, J.  
417 Geophys. Res. Atmos., 120, 5895–5909, doi:10.1002/2015JD023225, 2015.
- 418 Ding, Y. H., and Liu, Y. J.: Analysis of long-term variations of fog and haze in China  
419 in recent 50 years and their relations with atmospheric humidity, Sci. China  
420 Earth Sci., 57, 36–46, 2014.
- 421 Emanuel, K. A.: A scheme for representing cumulus convection in large-scale models,  
422 J. Atmos. Sci., 48, 2313–2329, 1991.
- 423 Gao, G.: The climatic characteristics and change of haze days over China during  
424 1961–2005, Acta Geogr. Sin., 63, 762–768, 2008.
- 425 Gao, X., Shi, Y., Zhang, D., Wu, J., Giorgi, F., Ji, Z., and Wang, Y.: Uncertainties in  
426 monsoon precipitation projections over China: results from two high-resolution  
427 RCM simulations, Clim. Res., 52, 213–226, 2012.
- 428 Gao, X., Shi, Y., and Giorgi, F.: Comparison of convective parameterizations in  
429 RegCM4 experiments over China with CLM as the land surface model, Atmos.  
430 Ocean. Sci. Lett., 9, 246–254, 2016a.
- 431 Gao, X., Shi, Y., Han, Z., Wang, M., Wu, J., Zhang, D., Xu, Y., and Giorgi, F.:  
432 Performance of RegCM4 over major river basins in China, Adv. Atmos. Sci.,  
433 doi:10.1007/s00376-016-6179-7, 2016b.
- 434 Giorgi, F., Jones, C., and Asrar, G.: Addressing climate information needs at the  
435 regional level: the CORDEX framework, WMO Bull., 58, 175–183, 2009.



- 436 Giorgi, F., Coppola, E., Solmon, F., Mariotti, L., Sylla, M., Bi, X., Elguindi, N., Diro,  
437 G., Nair, V., Giuliani, G., Turuncoglu, U., Cozzini, S., Güttler, I., O'Brien, T.,  
438 Tawfik, A., Shalaby, A., Zakey, A., Steiner, A., Stordal, F., Sloan, L., and  
439 Brankovic, C.: RegCM4: model description and preliminary tests over multiple  
440 CORDEX domains, *Clim. Res.*, 52, 7–29, 2012.
- 441 Guo, H., Xu, M., and Hu, Q.: Changes in near-surface wind speed in China: 1969–  
442 2005, *Int. J. Climatol.*, 31, 349–358, 2011.
- 443 Han, Z., Gao, X., Shi, Y., Wu, J., Wang, M., and Giorgi, F.: Development of Chinese  
444 high resolution land cover for the RegCM4/CLM and its impact on regional  
445 climate simulation (in Chinese), *Journal of Glaciology and Geocryology*, 37,  
446 857–866, 2015.
- 447 He, H., Wang, X. M., Wang, Y. S., Wang, Z. F., Liu, J. G., Chen, Y. F., 2013:  
448 Formation mechanism and control strategies of haze in China (in Chinese), *Bull.*  
449 *Chinese Acad. Sci.*, 28(3), 344–352.
- 450 Holtslag, A. A. M., De Bruijn, E. I. F., and Pan, H. L.: A high resolution air mass  
451 transformation model for short-range weather forecasting, *Mon. Wea. Rev.*, 118,  
452 1561–1575, 1990.
- 453 IPCC: Climate Change 2013: The Physical Science Basis. Contribution of Working  
454 Group I to the Fifth Assessment Report of the Intergovernmental Panel on Climate  
455 Change, Cambridge University Press, Cambridge, United Kingdom and New  
456 York, NY, USA, 1535pp, 2013.



- 457 Jacob, D. J., and Winner, D. A.: Effect of climate change on air quality, Atmos.  
458 Environ., 43, 51-63, 2009.
- 459 Jiang, Y., Luo, Y., and Zhao, Z. C.: Maximum wind speed changes over China, Acta  
460 Meteorol. Sin., 27, 63–74, 2013.
- 461 Kang, Z., Gui, H., Hua, C., Zhang, B., Zhang, H., Lv, M., and Wang, J.: National  
462 Environmental Meteorological Services in China, Adv. Meteorol., 2016, doi:  
463 10.1155/2016/1985207, 2016.
- 464 Kendall, M. G.: Rank Correlation Methods. Griffin, London, 1975.
- 465 Kiehl, J., Hack, J., Bonan, G., Boville, B., Williamson, D., and Rasch, P.: The  
466 National Center for Atmospheric Research Community Climate Model: CCM3, J.  
467 Clim., 11, 1131–1149, 1998.
- 468 Krishnan, P., and Kunhikrishnan, P.: Temporal variations of ventilation coefficient at  
469 a tropical Indian station using UHF wind profiler, Curr. Sci, 86, 447–451, 2004.
- 470 Lee, J., and Hong, S.: Potential for added value to downscaled climate extremes over  
471 Korea by increased resolution of a regional climate model, Theor. Appl.  
472 Climatol., 117, 667–677, 2014.
- 473 Leung, L. R., and Gustafson, W. I.: Potential regional climate change and  
474 implications to US air quality, Geophys. Res. Lett., 32, L16711, 2005.
- 475 Li, Q., Zhang, R. H., and Wang, Y.: Interannual variation of the winter-time fog–haze  
476 days across central and eastern China and its relation with East Asian winter  
477 monsoon, Int. J. Climatol., 36, 346–354, doi:10.1002/joc.4350, 2015.





- 478 Liu, J., and Diamond, J.: China's environment in a globalizing world, *Nature*, 435,  
479 1179–1186, 2005.
- 480 Mann, H. B.: Nonparametric tests against trend, *Econometrica*, 13, 245-259, 1945.
- 481 Oleson, K., Niu, G. Y., Yang, Z. L., Lawrence, D., Thornton, P., Lawrence, P.,  
482 Stöckli, R., Dickinson, R., Bonan, G., and Levis, S.: Improvements to the  
483 Community Land Model and their impact on the hydrological cycle, *J. Geophys.*  
484 *Res.*, 113, G01021, 2008.
- 485 Pal, J. S., Small, E. E., and Eltahir, E. A. B.: Simulation of regional-scale water and  
486 energy budgets: Representation of subgrid cloud and precipitation processes  
487 within RegCM, *J. Geophys. Res.*, 105, 29579–29594, 2000.
- 488 Park, T. W., Deng, Y., and Cai, M.: Feedback attribution of the El Niño–Southern  
489 Oscillation–related atmospheric and surface temperature anomalies, *Journal of*  
490 *Geophysical Research: Atmospheres*, 117, D23101, doi:10.1029/2012jd018468,  
491 2012.
- 492 Sen, P. K.: Estimates of the regression coefficient based on Kendall's tau, *Journal of*  
493 *the American Statistical Association*, 63, 1379-1389, 1968.
- 494 Song, L. C., Gao, R., Li, Y., and Wang, G. F.: Analysis of China's haze days in the  
495 winter half-year and the climatic background during 1961–2012, *Adv. Clim.*  
496 *Change Res.*, 5, 1–6, 2014.
- 497 Taylor, K. E., Stouffer, B. J., and Meehl, G. A.: An overview of CMIP5 and the  
498 experiment design, *Bull. Am. Meteorol. Soc.*, 93, 485–498, 2012.



- 499 Theil, H.: A rank-invariant method of linear and polynomial regression analysis,  
500 Proceedings of the Royal Netherlands Academy of Sciences, 53, I: 386–392, II:  
501 521–525, III: 1397–1412, 1950.
- 502 Tian, D., Guo, Y., and Dong, W. J.: Future changes and uncertainties in temperature  
503 and precipitation over China based on CMIP5 models. *Adv. Atmos. Sci.*, 32,  
504 487–496, doi:10.1007/s00376-014-4102-7, 2015.
- 505 Uppala, S., Dee, D., Kobayashi, S., Berrisford, P., and Simmons, A.: Towards a climate  
506 data assimilation system: Status update of ERA-Interim, *ECMWF newsletter*, 115,  
507 12–18, 2008.
- 508 Wang, H. J. and Chen, H. P.: Understanding the recent trend of haze pollution in  
509 eastern China: roles of climate change, *Atmos. Chem. Phys.*, 16, 4205–4211,  
510 doi:10.5194/acp-16-4205-2016, 2016.
- 511 Wang, H. J., Chen, H. P., and Liu, J. P.: Arctic sea ice decline intensified haze  
512 pollution in eastern China, *Atmos. Ocean. Sci. Lett.*, 8, 1–9, 2015.
- 513 Wang, H. J., He, S. P., and Liu, J. P.: Present and future relationship between the East  
514 Asian winter monsoon and ENSO: Results of CMIP5, *J. Geophys. Res. Ocean*,  
515 118, 1–16, doi:10.1002/jgrc.20332, 2013a.
- 516 Wang, X. P. and Mauzerall, D. L.: Evaluating impacts of air pollution in China on  
517 public health: implications for future air pollution and energy policies, *Atmos.*  
518 *Environ.*, 40, 1706–1721, 2006.



- 519 Wang, Y. S., Yao, L., Liu, Z. R., Ji, D. S., Wang, L. L., and Zhang, J. K.: Formation of  
520 haze pollution in Beijing-Tianjin-Hebei region and their control strategies, Bull.  
521 Chinese Acad. Sci., 28, 353–363, 2013b.
- 522 Wang, Z. F., Li, J., Wang, Z., Yang, W. Y., Tang, X., Ge, B. Z., Yan, P. Z., Zhu, L. L.,  
523 Chen, X. S., Chen, H. S., Wang, W., Li, J. J., Liu, B., Wang, X. Y., Wang, W.,  
524 Zhao, Y. L., Lu, N., and Su, D. W.: Modeling study of regional severe hazes  
525 over Mid-Eastern China in January 2013 and its implications on pollution  
526 prevention and control, Sci. China: Earth Sci., 57, 3–13,  
527 doi:10.1007/s11430-013-4793-0, 2014.
- 528 Wu, D., Tie, X., Li, C. C., Ying, Z. M., Lau, A. K., Huang, J., Deng, X. J., and Bi, X.  
529 Y.: An extremely low visibility event over the Guangzhou region: A case study,  
530 Atmos. Environ., 39, 6568–6577, 2005.
- 531 Wu, D., Liao, G. L., Deng, X. J., Bi, X. Y., Tan, H. B., Li, F., Jiang, C. L., Xia, D.,  
532 and Fan, S. J.: Transport condition of surface layer under haze weather over the  
533 Pearl River Delta, J. Appl. Meteorol. Sci., 19, 1–9, 2008.
- 534 Wu, J., Gao, X., Xu, Y., and Pan, J.: Regional climate change and uncertainty analysis  
535 based on four regional climate model simulations over China, Atmospheric and  
536 Oceanic Science Letters, 8, 147-152, 2015a.
- 537 Wu, J., Zhou, B. T., and Xu, Y.: Response of precipitation and its extremes over  
538 China to warming: CMIP5 simulation and projection, Chinese J. Geophys., 58,  
539 3048-3060, doi: 10.6038/cjg20150903, 2015b.



- 540 Xu, D., and Zhu, R.: A study on the distribution of ventilation and rainout capacity in  
541 mainland China (in Chinese), *China Environ. Sci.*, 9, 367-374, 1989.
- 542 Xu, P., Chen, Y. F., and Ye, X. J.: Haze, air pollution, and health in China, *Lancet*,  
543 382, 2067, doi:10.1016/S0140-6736(13)62693-8, 2013.
- 544 Xu, Y., and Xu, C. H., Preliminary assessment of simulations of climate changes over  
545 China by CMIP5 multi-models, *Atmos. Ocean. Sci. Lett.*, 5, 489–494, 2012.
- 546 Yin, Z. C., Wang, H. J., and Guo, W. L.: Climatic change features of fog and haze in  
547 winter over North China and Huang-Huai Area, *Sci. China Earth Sci.*, 58, 1370–  
548 1376, 2015.
- 549 Zhang, R. H., Li, Q., and Zhang, R. N.: Meteorological conditions for the persistent  
550 severe fog and haze event over eastern China in January 2013, *Sci. China: Earth  
551 Sci.*, 57, 26–35, 2014.



552 **Captions:**

553 **Table 1.** Statistic results for the simulation skills in annual mean AEC for the period  
554 of 1986-2005.

555 **Table 2.** Statistic results for the ensemble simulation skills in seasonal AEC for the  
556 period of 1986-2005.

557 **Table 3.** The consistence of the three ensemble members on the direction of the  
558 projected change over the four economic zones of China. Consistent projection  
559 on the decrease in AEC is marked by  $\surd$  and that on the increase in WVD is  
560 marked by  $\star$ .

561 **Table 4.** Trends of AEC and WVD (%/10a) over the four economic zones of China,  
562 based on 9-year running mean time series of the percentage change during  
563 2016-2099. Asterisks indicate the trends are statistically significant above the 95%  
564 confidence level.

565 **Figure 1.** Spatial distribution of annual AEC (unit:  $10^4\text{t/a/km}$ ) during 1986-2005: (a)  
566 observation, (b) ensemble, (c) EC, (d) HAD, (e) MPI.

567 **Figure 2.** Spatial distribution of seasonal AEC (unit:  $10^4\text{t/a/km}$ ) during 1986-2005:  
568 (a-b) winter, (c-d) spring, (e-f) summer, (g-h) autumn. Left panel is for the  
569 observation and the right panel is for the ensemble simulation.

570 **Figure 3.** Spatial distribution of (a-b) the number of weak ventilation days per year  
571 and (c-d) wet deposition (unit:  $10^4\text{t/a/km}$ ) during 1986-2005: (a, c) observation,  
572 (b, d) ensemble simulation.



573 **Figure 4.** Ensemble projected percentage changes (relative to 1986-2005) in (a-b)  
574 AEC and (c-d) WVD during (a, c) 2046-2065 and (b, d) 2080-2099. Hatched  
575 regions indicate all ensemble members agree on the sign of change.

576 **Figure 5.** Range of projected percentage changes (relative to 1986-2005) in (a) AEC  
577 and (b) WVD during 2046-2065 and 2080-2099, and 9a running mean time series  
578 of percentage changes in (c) annual, (d) winter (DJF), (e) spring (MAM), (f)  
579 summer (JJA), (g) autumn (SON) for the Beijing-Tianjin-Hebei region. In Figure  
580 (a-b), the bars represent the ensemble projection and the marks represent the  
581 individual projection of the three members; the left (right) bar in each group is for  
582 2046-2065 (2080-2099). In Figure (c-g), the solid (dashed) lines represent  
583 changes in AEC (WVD).

584 **Figure 6.** Same as Figure 5, but for Northeast China.

585 **Figure 7.** Same as Figure 5, but for Yangtze River Delta economic zone.

586 **Figure 8.** Same as Figure 5, but for Pearl River Delta economic zone.

587 **Figure 9.** Relative contributions (unit: %) of individual components to annual AEC  
588 change in the middle of the 21st century based on the ensemble results. (a)  
589 precipitation, (b) ventilation, (c) wind speed averaged with the boundary layer, (d)  
590 boundary layer depth, (e) nonlinear term, (f) transient term.

591 **Figure 10.** Relative contributions (unit: %) of individual components to annual AEC  
592 change in the middle of the 21st century averaged over four main economic  
593 zones of China: (a) BTH, (b) NEC, (c) YRD, (d) PRD. The bars represent the  
594 ensemble projection and the marks represent the individual projection of the three



595 members. Bars from left to right in each group are in turn for annual, DJF, MAM,  
596 JJA, and SON.



597 **Table 1.** Statistic results for the simulation skills in annual mean AEC for the period  
598 of 1986-2005.

Simulations	Pattern correlation coefficient (CC)	Root mean square error (RMES)
EC	0.76	0.47
HAD	0.79	0.54
MPI	0.75	0.48
Ensemble	0.77	0.49

599





600 **Table 2.** Statistic results for the ensemble simulation skills in seasonal AEC for the  
601 period of 1986-2005.

Season	Pattern correlation coefficient (CC)	Root mean square error (RMES)
Winter	0.79	0.76
Spring	0.75	0.68
Summer	0.61	0.56
Autumn	0.78	0.47

602



603 **Table 3.** The consistence of the three ensemble members on the direction of the  
 604 projected change over the four economic zones of China. Consistent projection on the  
 605 decrease in AEC is marked by  $\checkmark$  and that on the increase in WVD is marked by  
 606  $\star$ .

Economic zone	Period	ANN	DJF	MAM	JJA	SON
BTH	2046-2065	$\checkmark \star$	$\checkmark \star$		$\checkmark$	$\checkmark \star$
	2080-2099	$\checkmark \star$	$\star$			
NEC	2046-2065	$\checkmark \star$	$\checkmark \star$	$\star$	$\checkmark \star$	$\checkmark \star$
	2080-2099	$\checkmark \star$	$\checkmark \star$	$\checkmark \star$	$\checkmark \star$	$\checkmark \star$
YRD	2046-2065	$\checkmark \star$	$\checkmark \star$			
	2080-2099	$\star$	$\checkmark \star$			
PRD	2046-2065	$\star$		$\star$	$\star$	
	2080-2099	$\star$		$\star$	$\star$	

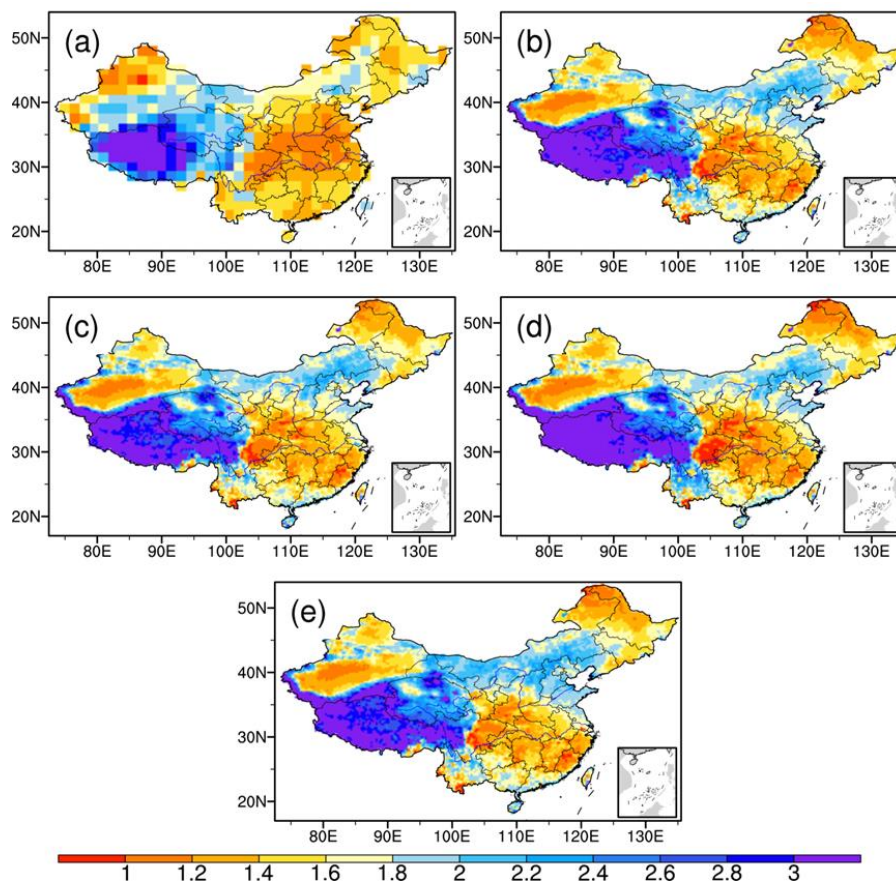
607



608 **Table 4.** Trends of AEC and WVD (%/10a) over the four economic zones of China,  
 609 based on 9-year running mean time series of the percentage change during 2016-2099.  
 610 Asterisks indicate the trends are statistically significant above the 95% confidence  
 611 level.

Economic zone	Variable	ANN	DJF	MAM	JJA	SON
BTH	AEC	-0.41*	-0.96*	0.02	-0.19*	-0.80*
	WVD	0.33	2.30*	-1.53*	-0.51*	0.55
NEC	AEC	-0.46*	-0.76*	-0.26*	-0.41*	-0.61*
	WVD	1.49*	2.60*	1.30*	0.73*	0.97*
YRD	AEC	-0.27*	-1.17*	0.32*	-0.45*	-0.02
	WVD	0.51*	0.88*	-0.26	0.71*	-0.15
PRD	AEC	-0.14*	-0.03	-0.22*	-0.12	-0.29*
	WVD	1.17*	-0.01	-0.30	2.17*	1.50*

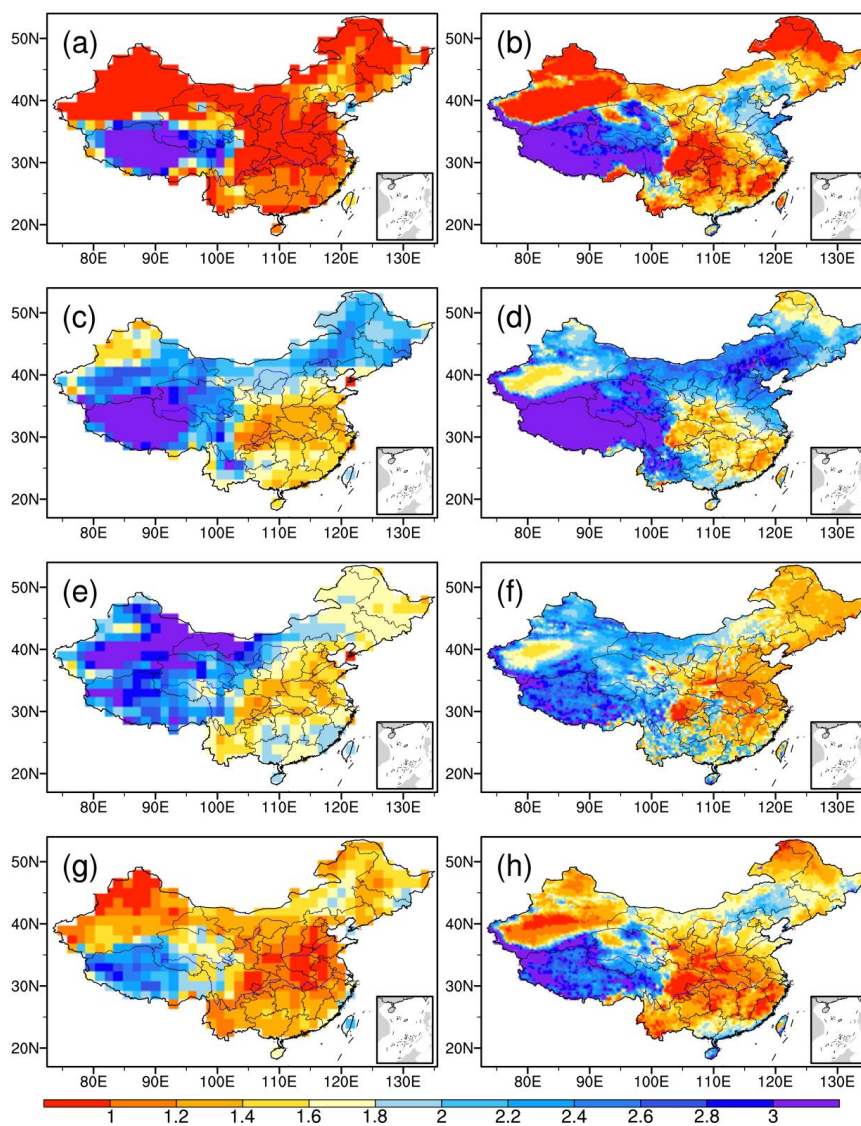
612



613

614 **Figure 1.** Spatial distribution of annual AEC (unit:  $10^4$  t/a/km) during 1986-2005: (a)

615 observation, (b) ensemble, (c) EC, (d) HAD, (e) MPI.

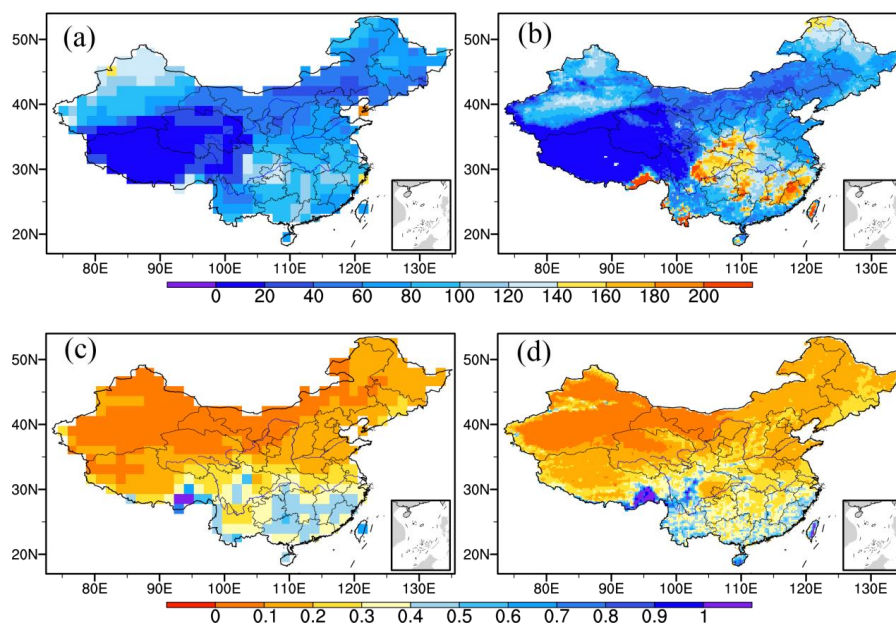


616

617 **Figure 2.** Spatial distribution of seasonal AEC (unit:  $10^4$ t/a/km) during 1986-2005:

618 (a-b) winter, (c-d) spring, (e-f) summer, (g-h) autumn. Left panel is for the

619 observation and the right panel is for the ensemble simulation.

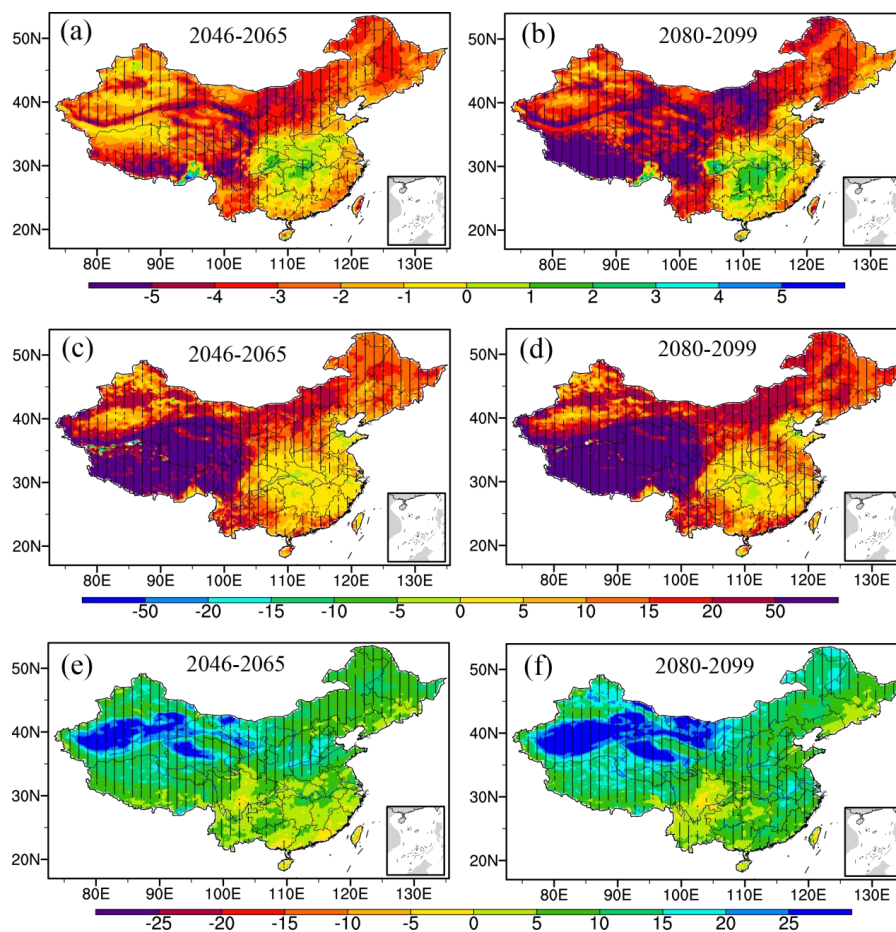


620

621 **Figure 3.** Spatial distribution of (a-b) the number of weak ventilation days per year

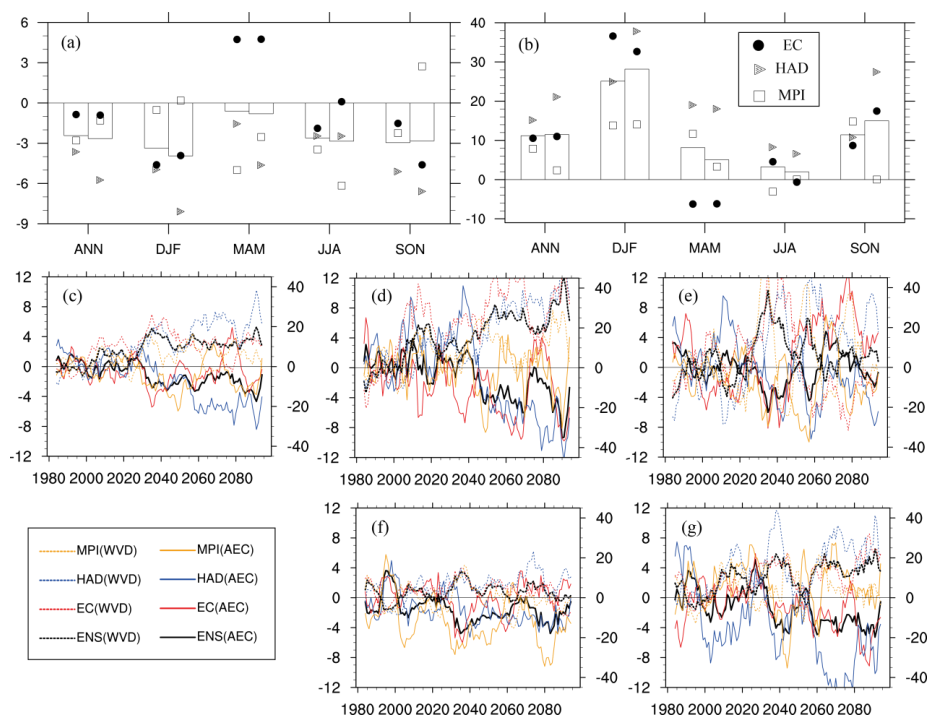
622 and (c-d) wet deposition (unit:  $10^4 \text{ t/a/km}$ ) during 1986-2005: (a, c) observation, (b, d)

623 ensemble simulation.



624

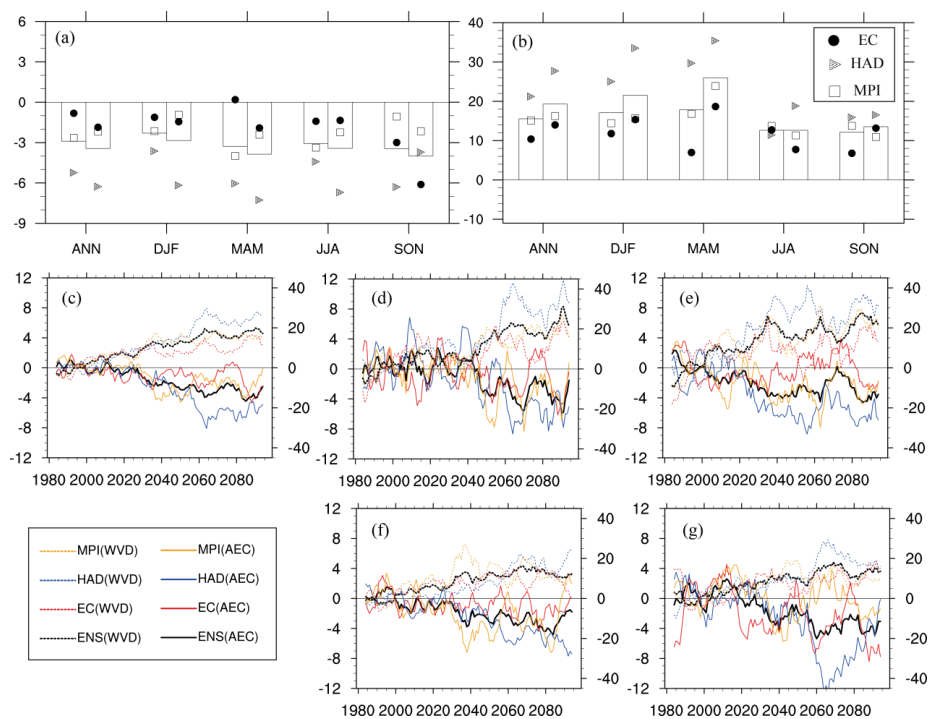
625 **Figure 4.** Ensemble projected percentage changes (relative to 1986-2005) in (a-b)  
626 AEC, (c-d) WVD, and (e-f) wet deposition during 2046-2065 (left panel) and  
627 2080-2099 (right panel). Hatched regions indicate all ensemble members agree on the  
628 sign of change.



629

630 **Figure 5.** Range of projected percentage changes (relative to 1986-2005) in (a) AEC  
631 and (b) WVD during 2046-2065 and 2080-2099, and 9a running mean time series of  
632 percentage changes in (c) annual, (d) winter (DJF), (e) spring (MAM), (f) summer  
633 (JJA), (g) autumn (SON) for the Beijing-Tianjin-Hebei region. In Figure (a-b), the  
634 bars represent the ensemble projection and the marks represent the individual  
635 projection of the three members; the left (right) bar in each group is for 2046-2065  
636 (2080-2099). In Figure (c-g), the solid (dashed) lines represent changes in AEC  
637 (WVD).

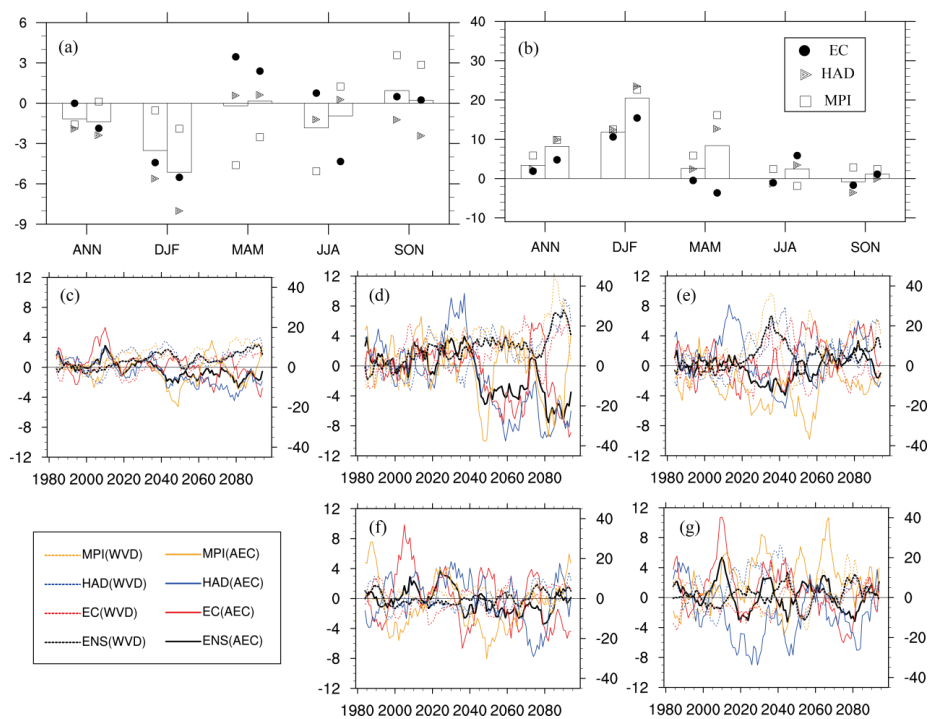




638

639

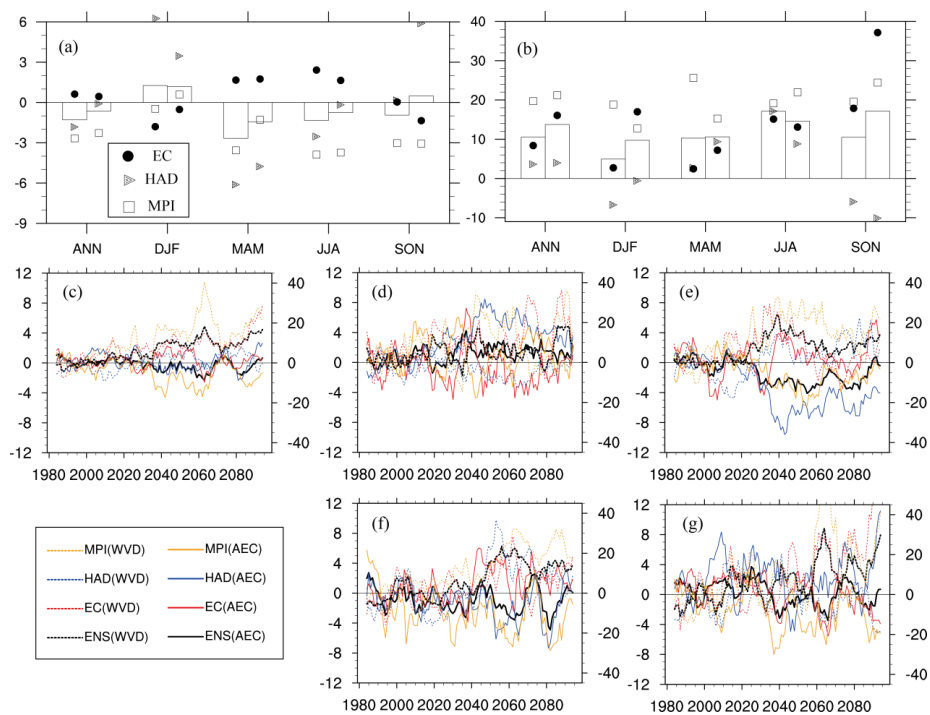
**Figure 6.** Same as Figure 5, but for Northeast China.



640

641

**Figure 7.** Same as Figure 5, but for Yangtze River Delta economic zone.

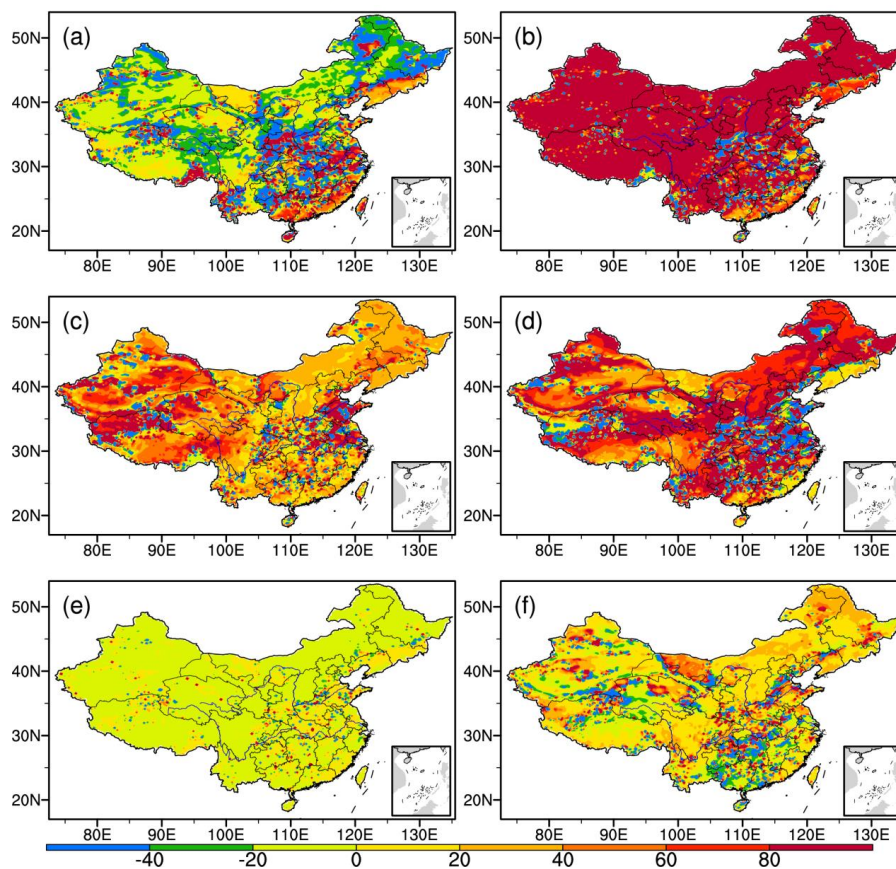


642

643

**Figure 8.** Same as Figure 5, but for Pearl River Delta economic zone.

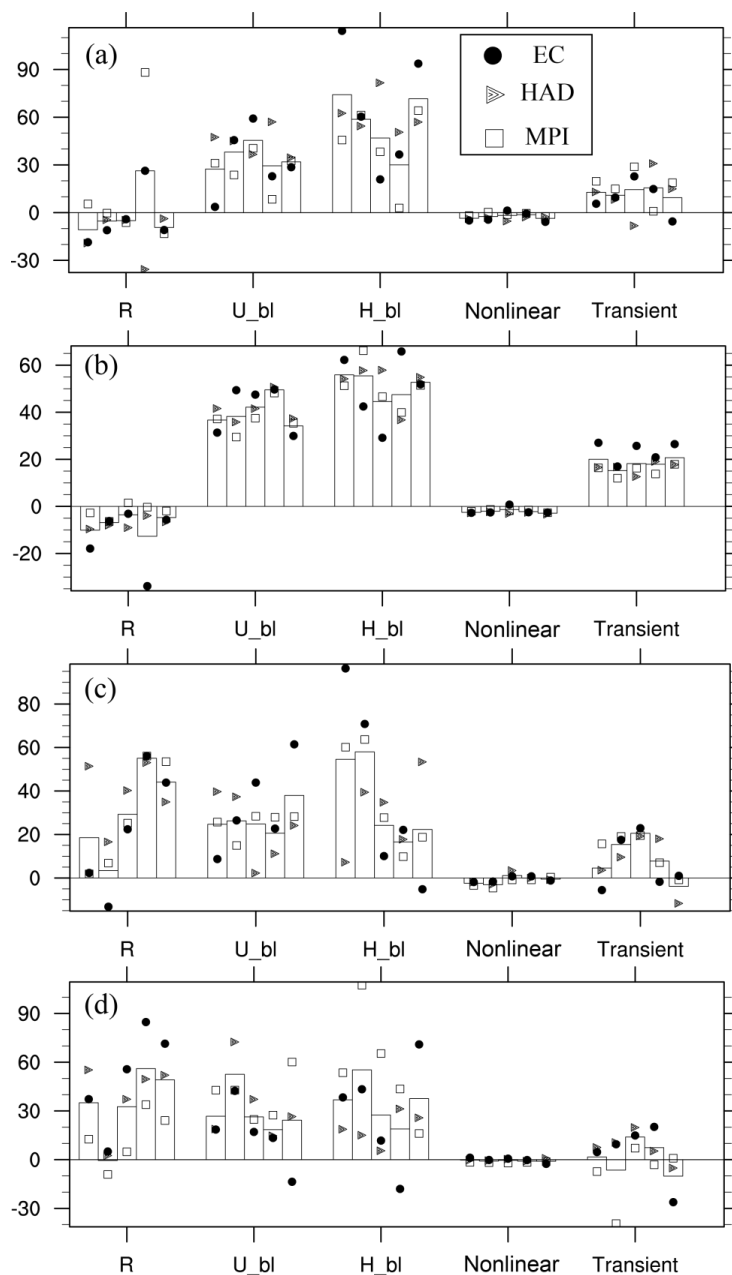
644



645

646 **Figure 9.** Relative contributions (unit: %) of individual components to annual AEC  
647 change in the middle of the 21st century based on the ensemble results. (a)  
648 precipitation, (b) ventilation, (c) wind speed averaged with the boundary layer, (d)  
649 boundary layer depth, (e) nonlinear term, (f) transient term.

650



651

652 **Figure 10.** Relative contributions (unit: %) of individual components to annual AEC

653 change in the middle of the 21st century averaged over four main economic zones of

654 China: (a) BTH, (b) NEC, (c) YRD, (d) PRD. The bars represent the ensemble



655 projection and the marks represent the individual projection of the three members.  
656 Bars from left to right in each group are in turn for annual, DJF, MAM, JJA, and  
657 SON.